European Journal of Cell Biology 104 (2025) 151519

Contents lists available at ScienceDirect

European Journal of Cell Biology

journal homepage: www.elsevier.com/locate/ejcb

Structure and function of the keratin 17 tail domain associated with keratin intermediate filament organization

Jiwoo Yeom [a], Sanghoon Lee [b], Young Ho Ko [c], Eunmi Hong [d], Jin Hae Kim [a,e,*], Pierre A. Coulombe [f,g,**], Chang-Hun Lee [a,e,*]

[a] Department of New Biology, Daegu Gyeongbuk Institute of Science and Technology, Republic of Korea
[b] Brain Research Core Facilities, Korea Brain Research Institute, Republic of Korea
[c] Center for van der Waals Quantum Solids, Institute for Basic Science, Pohang 37673, Republic of Korea
[d] New Drug Development Center, Daegu-Gyeongbuk Medical Innovation Foundation, Daegu. 41061, Republic of Korea
[e] New Biology Research Center, Daegu Gyeongbuk Institute of Science and Technology, Republic of Korea
[f] Department of Cell and Developmental Biology, University of Michigan Medical School, Ann Arbor, MI, USA
[g] Department of Dermatology, University of Michigan Medical School, Ann Arbor, MI, USA

ARTICLE INFO

Keywords:
Intermediate filament
Keratin
Filament bundling
Structure
Mechanical resilience
Nuclear Magnetic Resonance (NMR)
Intrinsically Disordered Region (IDR)

ABSTRACT

Keratins are the largest subgroup of intermediate filament proteins, forming 10-nm filaments from type I/II heterodimers, and occur primarily in epithelial cells. Keratin 6 (K6; type II) and Keratin 17 (K17; type I) show a complex expression pattern that includes induction following stress and in several diseases, including carcinomas. K17 is being used as a biomarker for several types of cancer. K6 and K17 sequences are respectively highly homologous to K5 and K14, which are expressed in the progenitor compartment of epidermis and related epithelia. The mechanical support roles of the K6/K17 and K5/K14 pairing require 10 nm filament assembly and the subsequent lateral association of these filaments to form thicker bundles. Previous studies showed that the non-helical tail domain of K14 is dispensable for 10 nm filament assembly but essential to the bundling of K5/K14 filaments. Whether the K6/K17 pairing undergoes bundling, and whether the tail domain of K17 plays a role, is unknown. Here, we use sedimentation assays and electron microscopy to show that, when paired with K6, tailless K17 forms filaments that do not readily bundle. Nuclear magnetic resonance analysis revealed that the isolated K17 tail domain is an intrinsically disordered region (IDR). Follow-up studies with mutant K17 tail constructs suggest that IDR-like tail domains of keratins can form a curved local structure required for bundling and interact dynamically with other regions of keratin filaments in a flexible and heterogeneous manner.

1. Introduction

The skin, the largest organ in the human body, provides a vital barrier against environmental factors, regulates body temperature, and facilitates sensory perception. Being at the interface between the body and the external environment, the skin possesses physical and chemical defense mechanisms that protects it against heat, pathogens, chemicals, and ultraviolet radiation. These protective functions rely in part on an intricate network of specialized proteins, including keratins, that together maintain skin structure and function under normal and stress conditions.

Keratins are intermediate filament (IF)-forming proteins and are particularly abundant in surface epithelia (Cohen et al., 2022). IFs are a crucial component of the cytoskeleton, forming a structural network within the cell that is attached at sites of cell-cell and cell-matrix adhesion and provides mechanical support, preserves cellular integrity, and contributes to many additional cellular processes (Kim and Coulombe, 2007; Windoffer et al., 2011; Seltmann et al., 2013). The significant contribution of IFs to cellular resilience is unique among cytoskeletal elements, complementing and extending the roles of F-actin and microtubules (Fuchs and Cleveland, 1998; Kim and Coulombe, 2007). Consequently, mutations or defects in IF sequences lead to diseases characterized by tissue fragility (Omary et al., 2004).

The IF superfamily includes ~70 genes that can be partitioned into 6

* Correspondence to: Department of New Biology, Daegu Gyeongbuk Institute of Science and Technology, Daegu, Republic of Korea.
** Corresponding author at: Department of Cell and Developmental Biology, University of Michigan Medical School, Ann Arbor, MI, USA.
E-mail addresses: jinhaekim@dgist.ac.kr (J.H. Kim), coulombe@med.umich.edu (P.A. Coulombe), leech@dgist.ac.kr (C.-H. Lee).

https://doi.org/10.1016/j.ejcb.2025.151519
Received 1 March 2025; Received in revised form 17 September 2025; Accepted 22 September 2025
Available online 26 September 2025

major subtypes based on gene substructure and sequence homology (Kim and Coulombe, 2007). With the exception of the type V nuclear lamins, IF proteins primarily occur in the cytoplasm, though exceptions to that general rule are emerging (Coulombe et al., 2024). All IF proteins possess three major and structurally distinct domains: the N-terminal head, the central rod, which is heptad repeat-rich and α-helical, and the C-terminal tail (Fig. 1A). Type I IF (n = 28) and type II IF (n = 26) genes code for keratin proteins, which are primarily expressed in epithelia and form 10-nm intermediate filaments from type I/II, coiled-coil heterodimers (Lee et al., 2012; Bunick and Milstone, 2017; Eldirany et al., 2019; Lee et al., 2020). Antiparallel, lateral interactions between heterodimers yield structurally apolar tetramers which then interact longitudinally and laterally to form protofibrils and, ultimately, mature 10-nm filaments (Fuchs and Weber, 1994). Several types of keratin filaments are capable of self-organization into cross-linked networks including bundles, which reflect lateral association between filaments to form thicker, multi-filamentous structures (Yamada et al., 2002; Lee and Coulombe, 2009). The formation of cross-linked networks is essential to achieve the mechanical properties required to support the structural role of keratin filaments in vivo (Ma et al., 2001; Lee and Coulombe, 2009; Alvarado and Coulombe, 2014).

The type I keratin (K17) and type II keratin 6 (K6) paralogs are significantly co-regulated in ectoderm-derived epithelial appendages (e.g., hair, nail, glands) and are co-induced or upregulated when complex epithelia are subjected to various stresses or undergo disease (McGowan and Coulombe, 1998; Cohen et al., 2024). Accordingly, these keratins are often referred to as "wound-inducible" or stress-responsive keratins (Zhang et al., 2019; Cohen et al., 2024). Upregulation of K6 and K17 occurs in a broad range of diseases, including psoriasis and cancers such as breast, cervical, oral squamous, and gastric carcinomas (Yang et al., 2018; Babu et al., 2019; Roa-Peña et al., 2019; Lin et al., 2022), and K17 levels have prognostic value for several carcinomas (Baraks et al., 2022; Delgado-Coka et al., 2024). Mutations in the K17 gene are also associated with steatocystoma multiplex and pachyonychia congenita

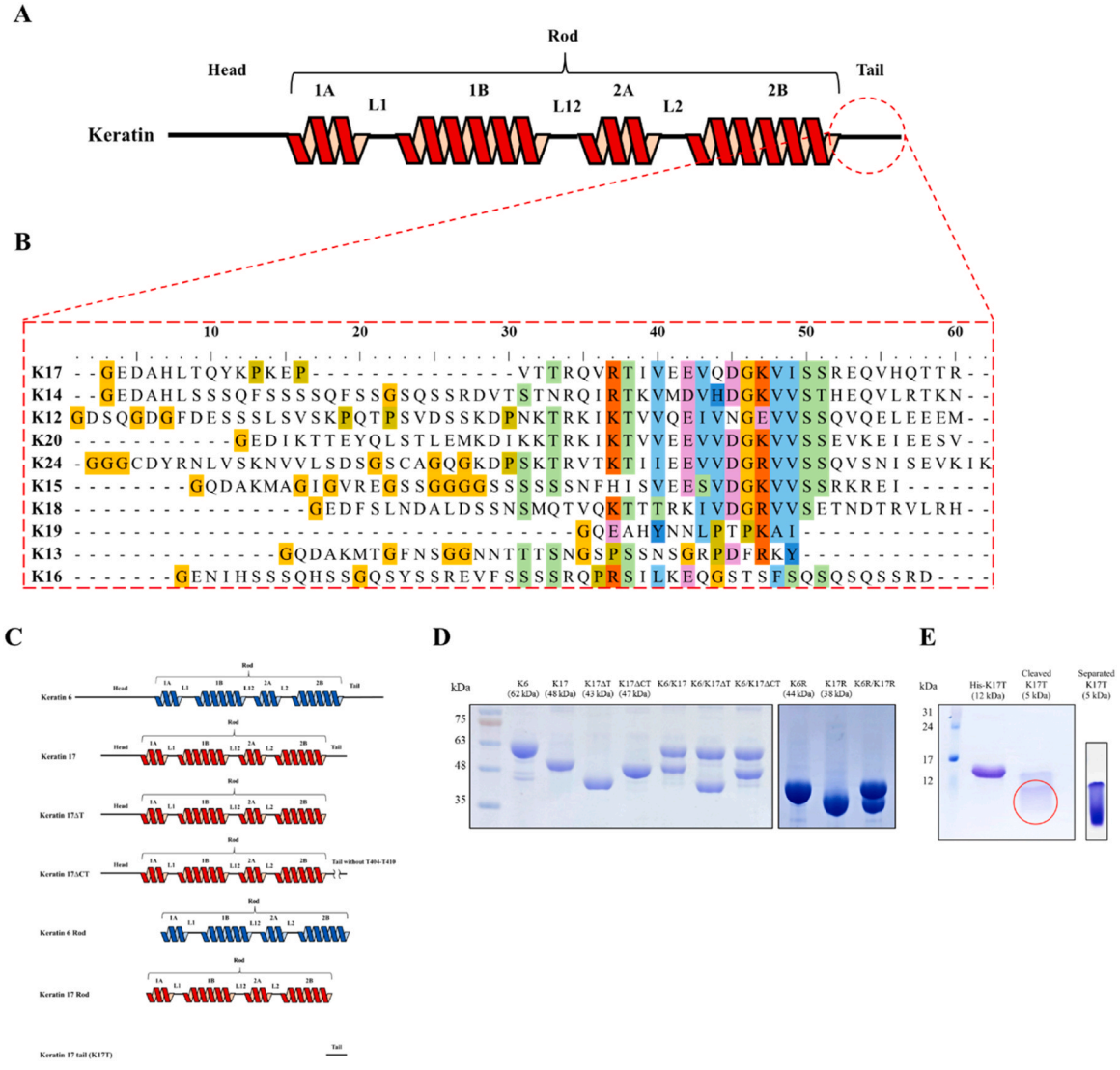

Fig. 1. Domain structure of keratin proteins. (A) Diagram of the keratin intermediate filament protein domains. Keratins consist of three major domains: head, rod, and tail. (B) Multiple sequence alignments for the tail domains of type I keratins. (C) Schematic of the recombinant K6, K17, K17ΔT, K17ΔCT, K6R, K17R, and K17T. (D) SDS-PAGE analysis of the recombinant keratins expressed in *E.coli*. Purified keratins were analyzed by gel electrophoresis (12 % SDS polyacrylamide) and visualized by staining with Coomassie brilliant blue. (Lane 1) wild-type K6; (Lane 2) wild-type K17; (Lane 3) K17ΔT; (Lane 4) K17ΔCT; (Lane 5) K6/K17 pair; (Lane 6) K6/K17ΔT pair; (Lane 7) K6/K17ΔCT pair; (Lane 8) K6R; (Lane 9) K17R; (Lane 10) K6R/K17R pair. (E) SDS-PAGE analysis of the recombinant K17T (K17 tail domain) expressed in *E.coli*. Purified K17T was analyzed using 18 % SDS polyacrylamide gel electrophoresis and visualized by staining with Coomassie brilliant blue. (Lane 1) His-tag infused K17T; (Lane 2) K17T cleaved by TEV protease. The red circle represents K17T part without His-tag; (Lane 3) Separated K17T using HiTrap Phenyl column.

(McLean and Lane., 1995; Liao et al., 2007; Gass et al., 2009; Zieman and Coulombe, 2020). In addition to its structural role, K17 regulates several signaling pathways involved in epithelial cell migration and cell growth (Coulombe and Wong, 2004; Chung et al., 2013) via interactions with the adaptor protein 14–3-3σ and the mTOR/AKT pathway (Kim et al., (2006); Khanom et al., (2016); Hobbs et al., (2016); Liu et al., (2020)), secretion of neutrophil chemokines (via regulation of Protein Kinase C alpha (PKCα) activity and signaling; Xu et al., (2024)), and hair follicle cycling (via TNFalpha-dependent apoptosis; Tong and Coulombe., 2006). The sequences of K6 and K17 are respectively highly homologous to keratin 5 (K5) and keratin 14 (K14), which are constitutively expressed in progenitor keratinocytes located in the basal layer of skin epithelia. The evidence in hand suggests that though homologous in several respects, K5/K14 and K6/K17 fulfill shared and distinct functions in skin keratinocytes (Cohen et al., 2024). A likely possibility is that such functional differences are specified, to a degree, by determinants located in the N-terminal head and C-terminal domains of these keratins, which are more divergent.

In this study, we show that the C-terminal tail domain of K17 (K17T), which is short (42 residues), is a key determinant of the ability of K6/K17 filaments to self-organize into bundles. Further, we employed nuclear magnetic resonance (NMR) spectroscopy to determine the structure of K17T, and show that it is highly disordered. Our findings suggest a key role for seven amino acid residues, located in the middle of the K17 tail domain, that maintain a curved structure to facilitate filament bundling. The structural model of the K17 tail domain provides a new perspective to understand structure-function relationships for type I keratins that exhibit conservation of this newly uncovered short structural motif.

2. Materials and methods

2.1. Plasmids

The keratin protein genes were subcloned into the following vectors for overexpression in *E.coli*: K6a (UniProt: P50446; pET-28b), K6 rod domain (K6R; from G133 to E473; pET-21), K17 (UniProt: Q9QWL7; pET-28b), K17 rod domain (K17R; from G83 to H394; pET-21), K17 tailless mutant (K17ΔT; from M1 to A393; pET-28b), K17 tail domain (K17T; from G390 to the end R433; pT7-HMT (Geisbrecht et al., 2006), and TEV protease (pET-15b-TEV-C9R, AddGene)). The DNA gene of the K17 deletion mutant of the curved tail region (K17ΔCT; full-length K17 internally deleted from T404 to T410) was synthesized and subcloned into pET-28b. All the genes used in this work were validated with sequencing. The boundary between the tail domain and the rod domain is based on the proteolytic experiment in the precedent literature (Lee and Coulombe, 2009). All keratin genes were synthesized based on codon-optimized sequences for *E.coli* expression (Bionics). Each plasmid was transformed into DH5α competent cells, and plasmid DNA was extracted using the AccuPrep Nano-Plus Plasmid Midi Extraction Kit (Bioneer) to ensure sufficient concentration for subsequent experiments.

2.2. Protein expression

The plasmids were transformed into Rosetta (DE3 pLysS) competent cells for keratin protein expression. Transformants were selected on LB agar plates containing ampicillin or kanamycin, depending on the plasmid resistance marker. Positive colonies were cultured in LB medium supplemented with the appropriate antibiotic. Protein expression was induced using 1 mM IPTG at 16°C for soluble proteins (K17 tail domain and TEV protease) and 37°C for insoluble proteins (K6a, K6R, K17, K17R, K17ΔT, and K17ΔCT). Following induction, the cells were incubated for an additional 16–20 h with shaking and harvested by centrifugation.

In the case of uniform ^{13}C and ^{15}N-labeling ([U-^{13}C; U-^{15}N]) for K17T, M9 minimal media (42.2 mM disodium phosphate, 22 mM potassium dihydrogen phosphate, 8.56 mM sodium chloride, 2 mM magnesium sulfate, 0.1 mM calcium chloride) with 0.4 % ^{13}C-glucose (Cambridge isotope) and 0.1 % ^{15}N-ammonium chloride (Cambridge isotope) was used instead of LB medium.

2.3. Inclusion body (IB) preparation

Expressed keratin proteins were isolated based on previously described methods (Bernot et al., 2005; Lee and Coulombe, 2009). Briefly, cell pellets were resuspended in lysis buffer (50 mM Tris-HCl, pH 8.0, 1 mM EDTA, 2 mM DTT, and 1 mM PMSF) and disrupted using a sonicator. After centrifuging the lysate (4°C, 20,000 ×*g*, 30 min), the pellet was washed with IB washing buffer I (50 mM Tris-HCl, pH 8.0, 0.2 M NaCl, 1 mM EDTA, 2 mM DTT, 1 mM PMSF, and 1 % NP-40) and centrifuged again. The pellet was washed with IB washing buffer II (50 mM Tris-HCl, pH 8.0, 0.5 M NaCl, 1 mM EDTA, 2 mM DTT, 1 mM PMSF, 0.5 % Triton X-100, and 0.5 % Tween-20), followed by centrifugation to obtain a purified inclusion body pellet.

2.4. Protein purification

The K6, K17 wild type, the K6 rod domain, the K17 rod domain, the tailless variant of keratin 17, and the curved tail region deleted mutant of keratin 17 were purified in multiple steps, including IB recovery, their solubilization and purification by ion-exchange chromatography using a HiTrap Q column (Cytiva). Equimolar type I and type II keratin pairs were purified using the HiTrap Q column followed by Mono Q column (Cytiva). Both columns used Buffer A (containing 6 M urea, 50 mM Tris-HCl (pH 8.0), 2 mM DTT, and 1 mM PMSF) and Buffer B (containing 6 M urea, 50 mM Tris-HCl (pH 8.0), 2 mM DTT, 1 mM PMSF, and 300 mM guanidinium chloride).

The fusion polypeptide of K17 tail domain with His-tag and Myc-tag (HMT-K17T) was purified via affinity chromatography using a HiTrap chelating column (Cytiva) with Buffer A containing 50 mM Tris-HCl (pH 8.0), 0.5 M NaCl, 5 mM imidazole, and Buffer B containing 50 mM Tris-HCl (pH 8.0), 0.5 M NaCl, 1 M imidazole. Additional purification was performed with a HiTrap Q column with Buffer A containing 25 mM Tris-HCl (pH 8.0) and Buffer B containing 25 mM Tris-HCl (pH 8.0), 1 M NaCl. The TEV protease, purified using a HiTrap SP column (Cytiva), was mixed with the HMT-K17T (1:25 ratio) and incubated overnight to cleave the His-tag and Myc-tag. The cleaved product was purified using a HiTrap Phenyl column (Cytiva) to separate the fusion tags or uncut HMT-K17T from the K17 tail domain. Buffer A contained 20 mM Tris-HCl (pH 7.5) and 1.5 M ammonium sulfate and Buffer B contained 20 mM Tris-HCl (pH 7.5).

2.5. Reconstitution of the keratin filament

Purified keratins were reconstituted into filaments through serial dialysis using the following buffer conditions: (a) 9 M urea, 25 mM Tris-HCl (pH 7.4), and 25 mM β-mercaptoethanol for 4 h at room temperature; (b) 2 M urea, 5 mM Tris-HCl (pH 7.4), and 5 mM β-mercaptoethanol for 4 h at 4°C; and (c) 5 mM Tris-HCl (pH 7.4) and 5 mM β-mercaptoethanol overnight at 4°C. The final buffer NaCl concentration was adjusted to 0 mM (standard assembly conditions) or 10 mM to promote network formation.

2.6. Assessing keratin filament assembly and bundling

Filament assemblies were evaluated using sedimentation assays (see Lee and Coulombe, 2009). To assess the efficiency of 10-nm filament polymerization, dialyzed samples (100 μL, 0.5 mg/mL) were subjected to ultracentrifugation (Airfuge, 100,000 × *g*, 1 h, room temperature). Pellets were resuspended in 20 μL sodium dodecyl sulfate (SDS) sample buffer (Biosesang) with 80 μL distilled deionized water (3DW). To assess the formation of bundled filament networks, a low-speed sedimentation

assay was conducted by centrifuging 100 µL of keratins (0.5 mg/mL, containing 10 mM NaCl) at 8000 × *g* for 30 min at 4°C to avoid any proteolytic damage to keratin proteins after adding NaCl and probable activation of contaminated protease(s). The pellet was resuspended in 20 µL SDS sample buffer with 80 µL of 3DW.

2.7. Electron microscopy and differential interference contrast microscopy

Filament assemblies were visualized with negative staining and transmission electron microscopy, as described (Lee and Coulombe, 2009). Protein samples (10 µL per sample) were applied to a copper grid and stained with 1 % uranyl acetate (Electron Microscopy Sciences). Samples were examined using a Tecnai G2 F20 TWIN TMP transmission electron microscope (FEI) operating at 200 kV.

Filament bundles were visualized with differential interference (DIC) microscopy, also described previously (Lee and Coulombe, 2009). Briefly, a keratin solution (30 µL per sample) was put on a glass slide with the barriers of hydrophobic nail polish solution. After adding NaCl solution to make a 10 mM concentration, a cover slip was put on the solution, and examined using an inverted microscope (Nikon Eclipse Ti-U) equipped with DIC optics module and S Plan Fluor ELWD 40x/0.60 DIC N1 lens.

2.8. NMR spectroscopy

For NMR experiments, [U-^{13}C; U-^{15}N]-K17T samples were prepared at a concentration of 0.34 mg/mL in a buffer containing 50 mM sodium phosphate (pH 7.4) and 7 % deuterium oxide (Cambridge isotope). The sample volume was adjusted to 300 µL and filled into a 5-mm Shigemi tube (Sigma-Aldrich). All NMR data were acquired on a Bruker Avance III HD 850 MHz spectrometer equipped with a cryogenic HCN probe (Bruker). The sample temperature was set to 283 K, the best condition for spectral quality in our screening trials. For the backbone signal assignment, we collected 2D ^{1}H-^{15}N heteronuclear single quantum coherence (HSQC), 3D HNCA, 3D CBCA(CO)NH, and 3D HNCACB spectra. Subsequent side-chain signal assignment was done with 2D ^{1}H-^{13}C HSQC, 3D HCCH-TOCSY, 3D ^{1}H–^{1}H NOESY ^{1}H-^{15}N HSQC, and 3D ^{1}H–^{1}H NOESY ^{1}H-^{13}C HSQC data sets. We used the TOPSPIN 3.2 software (Bruker) for data acquisition and processing, and the POKY software suite for additional data processing, signal assignment, and structure calculation (Lee et al., 2021).

Secondary structure and S^2 analyses were done by using TALOS-N (Shen and Bax, 2015) implemented in POKY. We used the POKY structure builder and the POKY analyzer for AUDANA/AUDASA-based NOESY spectral analysis, the XPLOR-based structural ensemble calculation, and the final structural model refinement (Schwieters et al., 2006; Lee et al., 2021, 2016). For the structural model calculation, we computed an ensemble of 200 potential models and selected the 20 lowest-energy models. The final ensemble was constructed with 17 models based on the structural consistency. Note that although the calculated ensemble of K17T exhibited significant disorder, we tabulated the statistics of the structural model calculation (Table 1), particularly for the residues presenting relatively high order parameters (T404-T410; Fig. 5B), to show the validity of our procedure and the final ensemble. Structural visualization and analysis were performed using PyMOL (DeLano, 2002).

The ensemble for the Table 1 was deposited to the Protein Data Bank (PDB) under accession code 9M1Y and the PDB DOI is 10.2210/pdb9m1y/pdb. The Biological Magnetic Resonance Bank (BMRB) code for this deposition is 36731 and the BMRB DOI is 10.13018/BMR36731.

2.9. DSS crosslinking assay followed by Western Blot

Cross-linking assays were performed using disuccinimidyl suberate (DSS; S1885; Sigma-Aldrich). DSS was dissolved in DMSO and added at a 20-fold molar excess relative to the protein concentration. After incubation for 30 min at room temperature, reactions were quenched with 200 mM Tris-HCl (pH 7.4). SDS was then added and samples were analyzed via SDS-PAGE.

Cross-linked protein samples were separated by SDS-PAGE and transferred to a 0.2 µm polyvinylidene fluoride (PVDF; AmershamTM HyBond P 0.2; Cytiva) membrane using a wet transfer system (100 V, 1 h). Membranes were blocked for 30 min at RT with 5 % skim milk in TBST buffer. Following the blocking step, membranes were incubated with a primary antibody (E-4) directed at an epitope from the K17 tail domain (sc-393002; Santa Cruz Biotechnology) diluted in TBST buffer (1:1000), overnight at 4°C. After incubation, membranes were washed three times for 10 min each with TBST buffer. Membranes were then incubated with a horseradish peroxidase (HRP)-conjugated secondary antibody (goat anti-Mouse IgG (H+L) 31430; Invitrogen) diluted in TBST buffer with 5 % skim milk (1:10,000) for 2 h at RT. After three additional washes in TBST buffer, the protein bands were visualized using an enhanced chemiluminescence (ECL; Pierce) detection system. Images were captured using a Chemiluminescence Imaging System (LuminoGraphI, ATTO Corporation, Japan).

Table 1
Summary of the parameters for modeled structures and NMR spectroscopy.

Analyses performed for well-defined residues.			
Total structures computed	200		
Number of structures used	17		
RMSD Values			
	all	ordered[e]	Selected[f]
All backbone atoms	8.4 Å	0.4 Å	0.4 Å
All heavy atoms	8.8 Å	1.4 Å	1.4 Å
Curvature forming region (T404-T410) backbone atoms	1.8 Å		
Structure Quality Factors - overall statistics			
	Mean score	SD	Z-score[g]
Procheck G-factor[e] (phi / psi only)	−0.51	N/A	−1.69
Procheck G-factor[e] (all dihedral angles)	−0.24	N/A	−1.42
Verify3D	−0.07	0.0229	−8.51
ProsaII (-ve)	−0.12	0.0608	−3.18
MolProbity clashscore	4.03	2.5113	0.83
Ramachandran Plot Summary from Procheck[f]			
Most favoured regions	98.50 %		
Additionally allowed regions	1.50 %		
Generously allowed regions	0.00 %		
Disallowed regions	0.00 %		
Ramachandran Plot Statistics from Richardson's lab			
Most favoured regions	100 %		
Allowed regions	0 %		
Disallowed regions	0 %		

[e]Residues with sum of phi and psi order parameters > = 1.8: Y401-E405
[f] Residues selected (DAOP with S(phi)+S(psi)> =1.8): Y401-E405
[g] With respect to mean and standard deviation for for a set of 252 X-ray structures < 500 residues, of resolution < = 1.80 Å, R-factor < = 0.25 and R-free < = 0.28; a positive value indicates a 'better' score.

3. Results

3.1. Purification of the keratin proteins

The following proteins were purified: full-length human K6 (K6); full-length human K17; K6 rod domain (K6R); K17 rod domain (K17R); a K17 variant lacking the tail domain (K17ΔT); and a K17 deletion mutant of the curved tail region (K17ΔCT) (Fig. 1C). These keratin proteins were first individually expressed in bacteria and then purified by ion-exchange chromatography under denaturing conditions (6 M urea-containing buffer). High-purity fractions were selected after initial purification, and equimolar amounts of K6 and K17, K6 and K17ΔT, or K6

and K17ΔCT were mixed and incubated overnight. The mixtures were purified using ion-exchange chromatography columns as described (Lee and Coulombe, 2009; see Fig. 1D). The keratin heterotypic complexes were separated on SDS polyacrylamide gels for visualization. After purification, the keratin complexes were dialyzed in 9 M → 2 M → 0 M urea-containing buffers to facilitate filament reconstitution. K17T was purified using His-tag affinity chromatography, and the His-tag was then cleaved and separated by TEV protease and hydrophobic interaction chromatography (Fig. 1E).

3.2. Sedimentation assay of the reconstituted keratin filaments

IF assembly and bundling were assessed using high-speed sedimentation and low-speed sedimentation assays, respectively (Bousquet et al., 2001; Lee and Coulombe, 2009). IFs that fail to properly assemble into long 10-nm filaments do not sediment when subjected to 100,000 × g ultracentrifugation for 1 h. In contrast, properly assembled filaments readily pellet in this setting. Thus, partitioning of the protein pool into the pellet and supernatant fraction reflects the extent of 10-nm filament assembly. On the other hand, centrifugation at 8000 × g (low-speed sedimentation) does not sediment individual, unbundled filaments. When filaments are part of a cross-linked network, e.g., bundles, the resulting assemblies will sediment under low-speed centrifugation conditions. Therefore, the pellet fraction after low-speed sedimentation serves as an indicator of the ability to undergo filament cross-linking.

To evaluate the assembly of reconstituted keratin pairs, high-speed sedimentation (100,000 × g, 1 h, room temperature) was performed, followed by SDS-PAGE analysis of the pellet and supernatant fractions (Fig. 2A and B). Both K6/K17 and K6/K17ΔT pairs were detected in the pellet fraction, regardless of the presence of NaCl, indicating highly efficient filament assembly (Fig. 2B). This result suggests that deletion of the K17 tail domain does not affect 10-nm filament assembly.

To assess keratin filament bundling, low-speed sedimentation was conducted in assembly buffer supplemented with 10 mM NaCl, which promotes filament bundling (Fig. 2C and D). Without NaCl, the K6/K17 and K6/K17ΔT pairs remained in the supernatant, indicating that bundling did not occur for either combination. In the presence of 10 mM NaCl, however, the K6/K17 pair predominantly sedimented into the

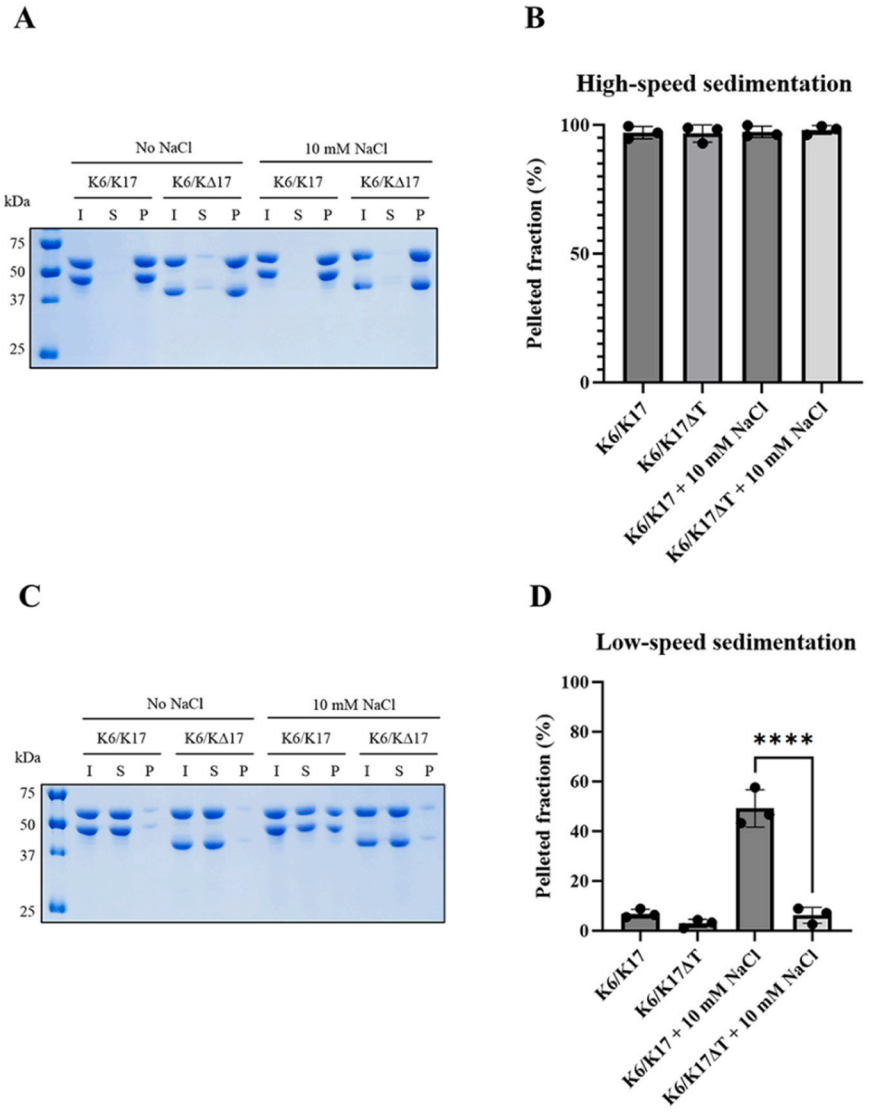

Fig. 2. Assessing filament assembly and bundling with sedimentation assays. (A) SDS-PAGE (12 % polyacrylamide gel) of the high-speed sedimentation assay. I: Input; P: Pellet; S: Supernatant. (B) Densitometry-based analysis of the pelleted fractions from (A). Pellet formation represents the assembly of keratin pairs. Data indicate mean ± SD (n = 3 per group). (C) SDS-PAGE (12 % polyacrylamide gel) of the low-speed sedimentation assay. I: Input, P: Pellet; S: Supernatant. (D) Densitometry-based analysis of the pelleted fraction from (C). Pellet formation represents the bundling of keratin pairs. Data indicate mean ± SD (n = 3 per group), one-way ANOVA, **** for $P < 0.0001$.

pellet fraction while most of the K6/K17ΔT pair remained in the supernatant (Fig. 2D). Thus, the K6/K17ΔT pairing did not give rise to cross-linked networks under conditions known to promote bundling, indicating that deleting the K17 tail domain abrogates this property.

3.3. TEM observations of the reconstituted keratin filaments

The outcomes of high-speed and low-speed sedimentation assays suggest that the deletion of K17T does not affect filament assembly but severely impairs the formation of cross-linked networks. To validate this interpretation and extend our analyses, we next sought to visualize the structural attributes of the filament assemblies using negative staining and TEM. After reconstitution, the keratin concentration was adjusted to 0.05 mg/mL, and TEM imaging was performed following negative staining. Both the K6/K17 and K6/K17ΔT pairs assembled into elongated filaments in the absence of NaCl, indicating efficient filament formation (Fig. 3A and B). Furthermore, even in the presence of 10 mM NaCl, both K6/K17 and K6/K17ΔT pairs continued to exhibit normal filament assembly (Fig. 3C and D). These TEM analyses, therefore, consistently support the sedimentation assay results, confirming that the deletion of K17T did not impair K6/K17 filament assembly.

3.4. Structural analysis of K17T using NMR

Using NMR data, the molecular structure of K17T was determined in an effort to elucidate the molecular mechanism by which K17T stabilizes K6/K17 filament bundling. 3D NMR experiments of a [U-^{13}C; U-^{15}N]-K17T sample were conducted to obtain a molecular structure of K17T. Before solving the complete structure, the backbone chemical shift data obtained during the structural analysis were used to predict the secondary structure and flexibility of K17T. Torsion Angle Likelihood Obtained from Shift and sequence similarity–Neural network (TALOS-N) was used for this analysis. TALOS-N is a powerful tool to predict the secondary structure by comparing the backbone chemical shift data from NMR experiments given access to existing high-resolution X-ray and NMR structural databases and identification of patterns that resemble known structures (Shen and Bax, 2015). The probability of each residue adopting an α-helix, β-strand, or loop (coil) conformation was determined. The central region (V408–V412) of K17T exhibited a higher probability of forming a β-strand, though only 40 %–60 %. The remaining residues were predominantly predicted to form loop structures (Fig. 4A). This analysis suggests that K17T is a highly disordered region with a minimally stable secondary structure.

Similar to the secondary structure prediction, the random coil index (RCI-S^2) evaluates the flexibility or stability of each amino acid residue by comparing the structure of the residue to a structural database. Lower RCI-S^2 values (<0.6) indicate greater disorder, flexibility, and structural instability. Higher values (>0.6) suggest more stable structures (Peck et al., 2024). Most residues of K17T had RCI-S^2 values near or below 0.6 (Fig. 4B). Combined with the secondary structure prediction, this data strongly suggests that K17T is an intrinsically disordered region (IDR).

Side-chain assignments and refinements were conducted to further assess the structure of K17T. The structural analysis confirmed that K17T exhibits clear characteristics of an IDR. Overall, K17T displays a highly flexible structure, with a less disordered core region (T404–T410) forming a curvature (Fig. 4C and D). Given such structural features, the overall flexibility may facilitate binding of the tail domain to the coiled-coil rod domains of keratin filaments while the curvature in the central region may play a crucial role in stabilizing filament bundling. The overall backbone RMSD (BB RMSD) of K17T was 8.4 Å, indicating significant flexibility. However, the curved region near the middle of K17T had a lower BB RMSD of 1.8 Å, suggesting that this portion maintains a relatively consistent conformation (Fig. 4C and D). The stabilized local structure in the curved region is formed by the local and consecutive intra-molecular interaction with van der Waals forces (Fig. 4E and F). These findings further support the idea that the structure of K17T is flexible, enabling dynamic interactions with keratin filaments, and the structured curvature region may act as a key element in filament

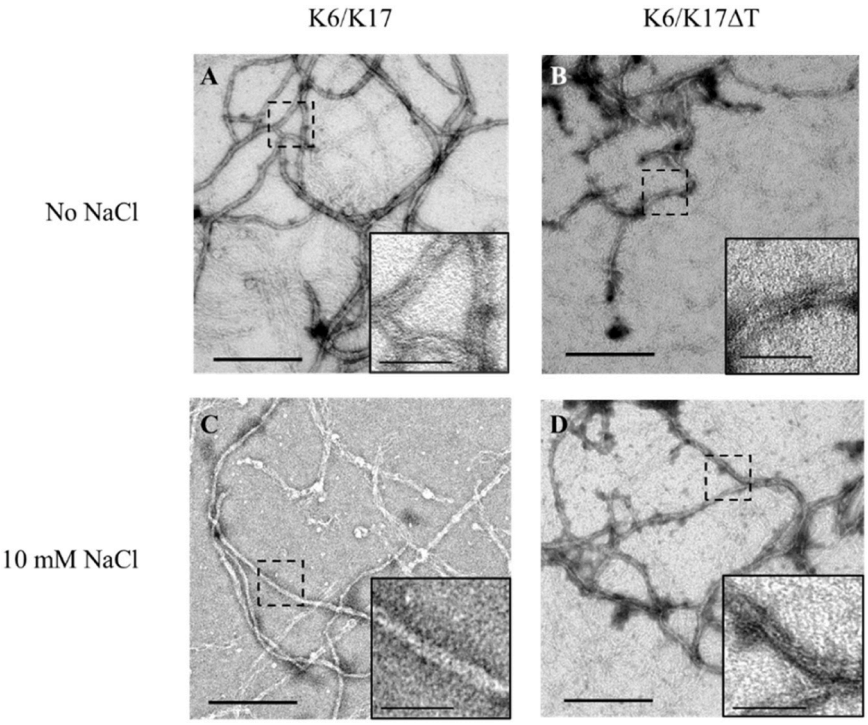

Fig. 3. Assembly of the tailless keratin filaments. Equimolar mixtures of type I and type II keratins were incubated in vitro and subjected to stepwise dialysis using serially diluted urea-containing buffers as described in Materials and Methods. After negative staining, assemblies were visualized using TEM. (A, B) Assembled keratin filaments of K6/K17 and K6/K17ΔT pairs without NaCl. (C, D) Assembled keratin filaments of K6/K17ΔT pairs with 10 mM NaCl. The scale bars represent 200 nm. The scale bars in the inset images represent 50 nm.

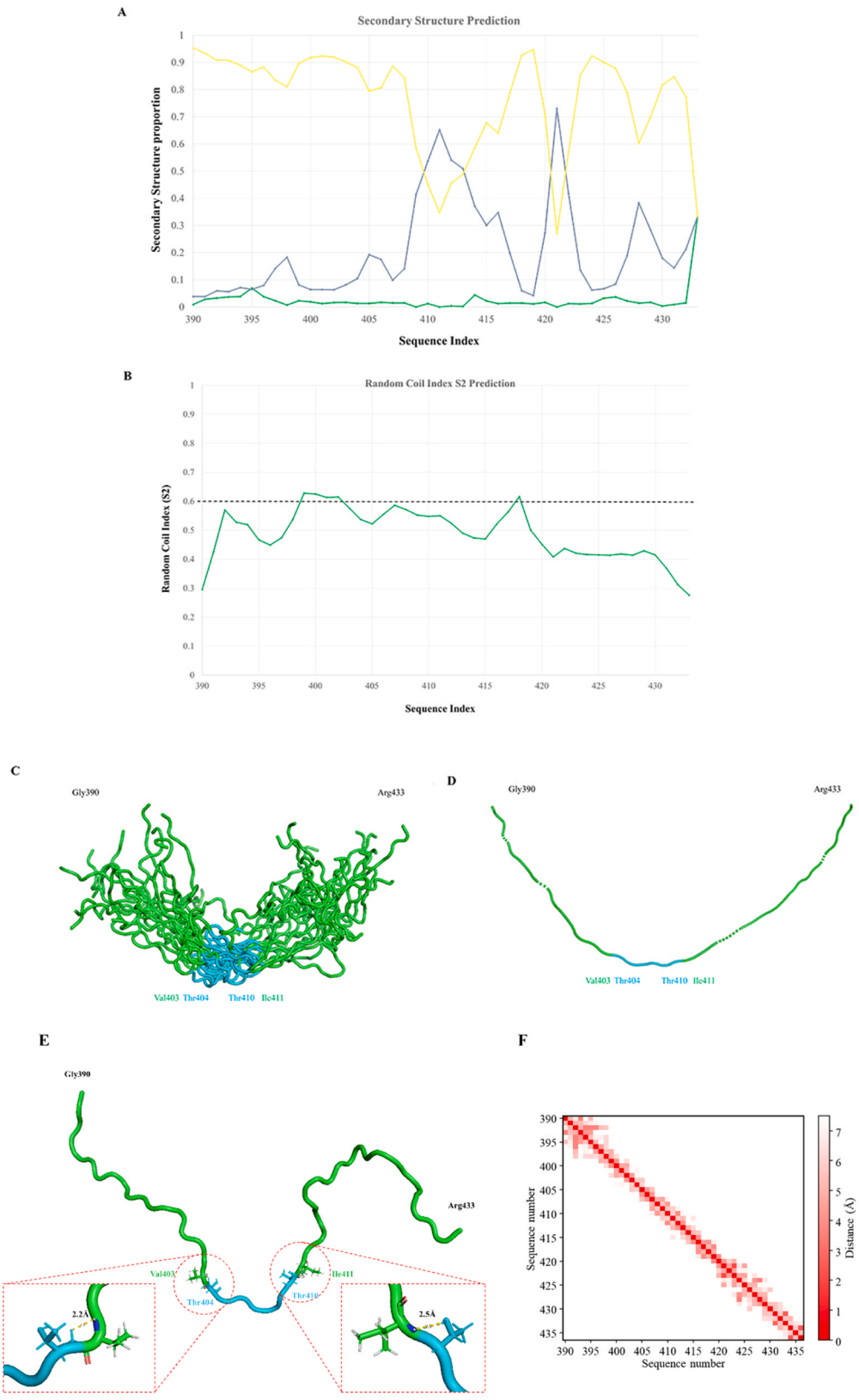

Fig. 4. Structural calculations using NMR. For the molecular structure of K17T NMR experiments with a [U-^{13}C; U-^{15}N]-K17T sample were conducted. (A) Secondary structure was predicted using TALOS-N with the chemical shift data of K17T. Green: helix, Blue: strand, Yellow: loop. (B) Predicted RCI-S^2 by TALOS-N with the chemical shift data of K17T. The threshold for stable structure is 0.6. (C) 17 structural models of K17T in solution. Cyan coloring highlights a consistently curved region, T404–T410. (PDB ID: 9M1Y). (D) Mean structure of the ensemble shown in (C). Again, cyan coloring highlights a consistently curved region, T404–T410. (E) Example of local structure seen in the models with lowest energies showing stabilizing intra-molecular interactions. (F) Contact map of the K17T based on the atomic distance between the residues.

bundling stabilization.

3.5. Conformational changes in K17T in response to alterations in buffer conditions

After establishing the crucial role of K17T in K6/K17 filament bundling, the mechanism by which K17T facilitates the bundling of fully assembled filaments was investigated. Tail-tail association was investigated first. Tail domains mostly extend outwardly in fully assembled keratin filaments, a reality first demonstrated for the K14 tail domain using partial proteolysis and MALDI-TOF mass spectrometry (Lee and Coulombe, 2009). The K14 and K17 tail domains show 41 % sequence identity, and share a rod domain-proximal (N-terminal) cleavage motif, 'GEDAHL'. From this, we infer that it is highly likely that the K17 tail domain similarly extends outward from the assembled filament. The recent cryoelectron tomography insight into the structure of vimentin filaments *in situ* (Eibauer et al., 2024) revealed that the tail domains of vimentin occer at the surface of the filaments, filling the spaces between the protofibrils. This suggests the possibility that tail domains exposed at the surface of assembled filaments may undergo structural change under the bundling-promoting buffer conditions.

Previous studies have reported that bundling of intermediate filaments (IFs), such as keratin and vimentin, can be induced by shifts in pH or the presence of divalent cations like Ca^{2+} and Mg^{2+} (Fukuyama et al., 1978; Wu et al., 2020). Therefore, the possibility of K17T conformational changes under these conditions was investigated using NMR spectroscopy. To investigate the effects of divalent metal cations, ^{1}H-^{15}N HSQC experiments on K17T in the presence of Ca^{2+} and Mg^{2+} were conducted. The K17T spectra showed no significant changes in the presence of Ca^{2+} or Mg^{2+} (Fig. 5 A), suggesting that it does not undergo conformational changes in the presence of divalent metal ions known to promote filament bundling. The effects of altering pH were investigated by observing changes in the ^{1}H-^{15}N HSQC spectra of K17T at pH 7.5 (non-bundling condition) and pH 6.8 (bundling condition). Lowering the pH to 6.8 did not induce significant changes in the spectra (Fig. 5B), suggesting that K17T does not undergo conformational changes in response to pH shifts during filament bundling stabilization.

Overall, these findings suggest that K17T neither possesses a binding site for divalent metal ions, nor undergoes pH-induced conformational changes. It implies that salt ion or pH-mediated change for filament bundling might take place in a tail binding site(s) of keratin protein, rather than the tail domain itself. This behavior is in contrast to the vimentin tail, which is known to interact with divalent cations to form networks (Wu et al., 2020).

3.6. K17 tail domain specifically binds to the K6 rod domain

Our structural and functional analyses suggested that the K17T is a crucial determinant of K6/K17 filament bundling. Based on these findings, we hypothesized that K17T mediates the bundling of K6/K17 filaments by binding directly to the rod domain of K6/K17. To test this hypothesis, we performed in vitro cross-linking experiments using the chemical cross-linker disuccinimidyl suberate (DSS) and Western blot using an antibody specific to the K17T sequence.

In the non-bundling condition (no NaCl), DSS treatment of the K6R and K17R mixture resulted in the formation of high-molecular-weight complexes, as shown by SDS-PAGE analysis (Fig. 6A). Western blot analysis using a K17T antibody revealed that K17T also binds to these complexes (Fig. 6B).

However, a significant change in the band patterns was observed under bundling-promoting buffer conditions (10 mM NaCl, 1 mM $CaCl_2$). The high-molecular-weight complexes formed by the K6R and K17R domains were reduced significantly. Furthermore, a new set of complex bands with a wider range of molecular weights (approximately 49 kDa, 87 kDa, 174 kDa) appeared (Fig. 6A). Comparison with the reference size marker bands suggests that K17T (5 kDa) specifically binds to the K6R (44 kDa + 5 kDa), rather than to K17R (38 kDa + 5 kDa). Also, the emergence of K17 T-associated bands suggests that K17 tail association with the K6 rod domain is likely enhanced by bundling-promoting buffer conditions (Fig. 6B).

These results provide strong evidence that the K17 tail domain specifically interacts with the K6 rod domain, and this interaction is influenced by bundling-promoting buffer conditions. This direct interaction between the K17T and the K6R provides a molecular mechanism for the observed tail-dependent filament bundling and the enhanced mechanical resilience of the K6/K17 filament network.

3.7. The curvature forming region (T404–T410) of K17T is essential for K6/K17 filament bundling

Our NMR-based structural analysis of K17T revealed an overall intrinsically disordered structure with a short and consistently curved core in its middle (T404–T410). We next hypothesized that this region is a key element for promoting and stabilizing K6/K17 filament bundling (Fig. 5). To experimentally validate the functional significance of this specific curvature, we engineered a K17 mutant where residues T404–T410 were deleted, designated K17ΔCT. We then conducted a comparative analysis of the filament assembly and bundling capacities of K6/K17ΔCT alongside wild-type K6/K17 and the tailless mutant (K6/K17ΔT), employing both high- and low-speed sedimentation assays, transmission electron microscopy, and differential interference contrast

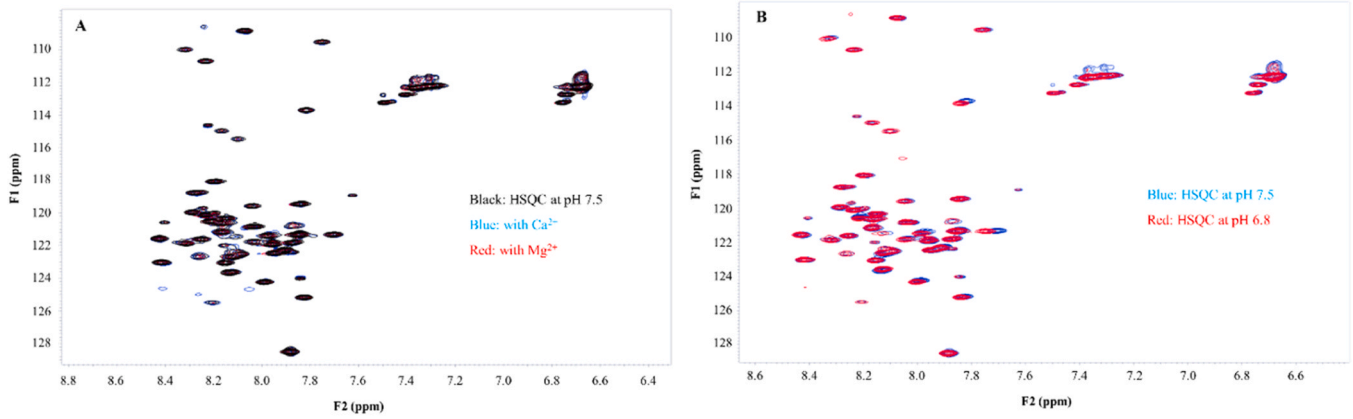

Fig. 5. ^{1}H-^{15}N HSQC of K17T after exposure to divalent metal ions or pH changes. (A) ^{1}H-^{15}N HSQC spectrum of K17T in the presence of 1 mM Ca^{2+} or 1 mM Mg^{2+} in 10 mM HEPES buffer (pH 7.5). Black: without divalent metal ion, Blue: with Ca^{2+}, Red: with Mg^{2+}. (B) ^{1}H-^{15}N HSQC spectrum of K17T at pH 7.5 and pH 6.8. Blue: pH 7.5. Red: pH 6.8.

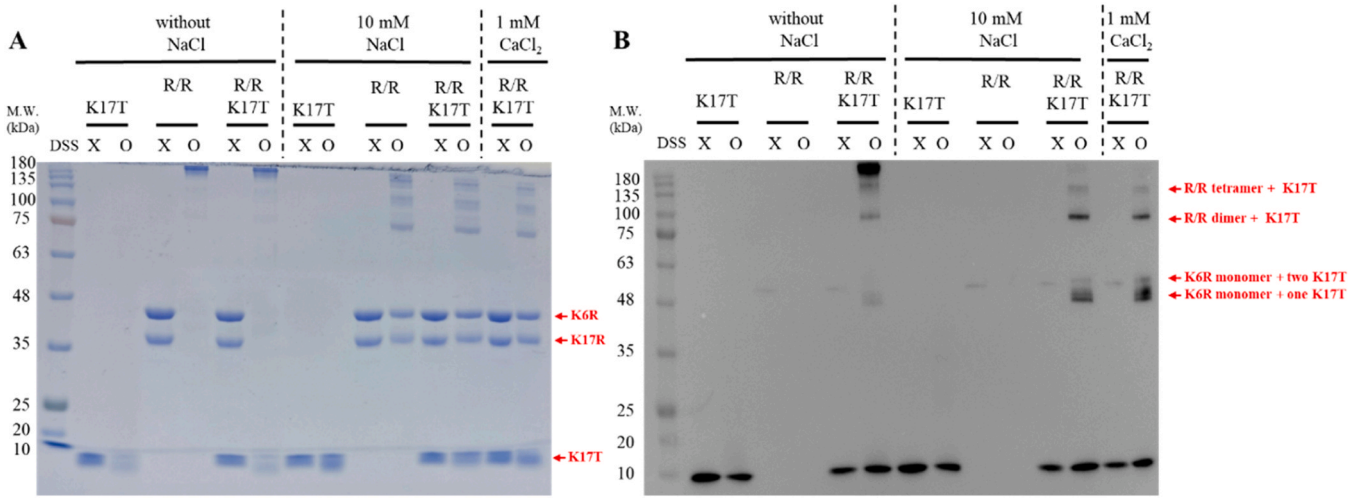

Fig. 6. K17 tail domain specifically interacts with the K6 rod domain *in vitro*. (A) SDS-PAGE (12 % polyacrylamide gel) of the DSS cross-linking assay between K17T and K6R/K17R complex (R/R). M.W. indicates the molecular weight by size markers. (B) Western blot analysis of the SDS-PAGE gel shown in (A), probed with an antibody specific for the K17T. R/R represents the heterocomplex of the rod domains, K6R/K17R.

(DIC) microscopy.

High-speed sedimentation assay results showed that K6/K17ΔCT assemblies, similar to the tailless mutant, pelleted readily, suggesting no impact on filament assembly capability (Fig. 7A and B). Conversely, in low-speed sedimentation assays performed under 10 mM NaCl conditions, the K17ΔCT mutant (like the tailless mutant) largely remained in the supernatant fraction while wild type K6/K17 assemblies partitioned to the pellet fraction (Fig. 7A and B). This suggests that the curvature-forming region plays a crucial role in bundling.

TEM was performed to investigate potential changes in filament morphology induced by the 7-residue deletion in K17T. Consistent with the sedimentation assay results, the K17ΔCT mutant still allowed for 10-nm filament assembly with or without 10 mM NaCl (Fig. 7C-H). A notable difference was that the K6/K17ΔCT group (14.91 nm ± 3.20 nm; n = 51) showed a thicker filament width compared to both the wild type (11.73 nm ± 1.42 nm; n = 51) and the tailless group (13.37 nm ± 2.26 nm; n = 51) (Fig. 7C-H). To provide an alternative approach to visualizing keratin filament bundle formation involving a large fraction of the samples, DIC microscopy was conducted. While K6/K17 wild-type readily formed relatively thick filament bundles (Fig. 7I), the K6/K17ΔT and K6/K17ΔCT mutants only formed very thin bundles (Fig. 7J and K). These analyses involving the K6/K17ΔCT mutant confirmed that the curved core region (T404-T410) seen by NMR microscopy is required to form K6/K17 keratin bundles.

4. Discussion

Formation of cross-linked networks significantly enhances the mechanical resilience of cytoskeletal networks (Pegoraro et al., 2017). Keratin filaments, in particular, are readily capable of self-organizing into bundles (Yamada et al., 2002; Lee and Coulombe, 2009; Alvarado and Coulombe, 2014; Ramms et al., 2013), a property that is key to their conferring mechanical resilience and integrity to epithelial cells and tissues by enabling them to withstand various forms of physical stress (e.g., compression, tension, shear forces). This mechanical robustness is essential for maintaining the epidermal barrier function and protecting against external damage (Alvarado and Coulombe, 2014; Ramms et al., 2013). For K5/K14 keratin filaments, it has been shown that the 1 A and 2B domains of K5 and the tail domain of K14 mediate filament bundling in vitro and in vivo (Lee and Coulombe, 2009; Alvarado and Coulombe, 2014). Whether the tail domain of other type I keratins possess similar properties is, however, unknown. The sequences of the tail domains in type I keratins can be highly divergent and have low complexity, and yet some of them share similar sequence motifs (Franke, 1987).

Our results show that the C-terminal tail domain of K17 (K17T) is crucial for K6/K17 filament bundling. High-speed sedimentation assays demonstrated that both K6/K17 and K6/K17ΔT pairs assemble into filaments, indicating that K17T is not essential for filament formation. However, low-speed sedimentation assays and DIC microscopy images revealed a significant reduction in bundling for the K6/K17ΔT pair compared to the wild-type K6/K17 pair, suggesting that K17T contributes to the bundling process. With TEM observations, both of the wild-type K6/K17 and K6/K17ΔT pairs exhibited well-assembled filaments. These findings are in agreement with previous observations from the K5/K14 keratin pair in which the K14 tail domain is critical for filament bundling, but not for assembly (Wilson et al., 1992; Bousquet et al., 2001; Lee and Coulombe, 2009).

K5/K14, constitutively expressed in basal keratinocytes, typically forms a highly organized and mechanically robust network that is essential for resisting constant physical stresses and maintaining the stable architecture of epithelial tissues (Kim and Coulombe, 2007; Ramms et al., 2013). In contrast, K6/K17 are stress-responsive keratins that are rapidly upregulated during dynamic processes like wound healing, inflammation, and hyperproliferation (Coulombe and Omary, 2002; Coulombe et al., 2024). It is known that the conserved region of the C-terminal K14 tail ("T2") is important for bundling formation, and K17T's C-terminal region is similar to the T2 region of the K14 tail domain (Lee and Coulombe, 2009; Fig. 1B). Given the high sequence homology among these keratins, similar tail-dependent bundling mechanisms probably exist across other type I/type II keratin pairs. Future studies should explore whether other type I keratins exhibit similar bundling dependencies through comparative structural and functional analyses.

To determine whether K17T undergoes conformational changes under conditions favorable for filament bundling conditions, ^{1}H-^{15}N HSQC experiments were performed in the presence of Ca^{2+} and Mg^{2+} and at pH 6.8. The K17T spectra did not change under these conditions, suggesting that self-dimerization and conformational changes induced by environmental factors do not occur during K17T-mediated stabilization of the K6/K17 filament bundling. Instead, K17T may interact with other segments of keratin proteins during the bundling process. During K5/K14 bundling, the C-terminal half of the K14T (T2 region) binds to the 1 A and 2B domains of K5 (Lee and Coulombe, 2009; Alvarado and Coulombe, 2014). If this also occurs during K6/K17 bundling, the T2 region of K17T may bind with the 1 A and 2B domains of K6. Our in vitro DSS cross-linking experiments provided evidence that K17T directly

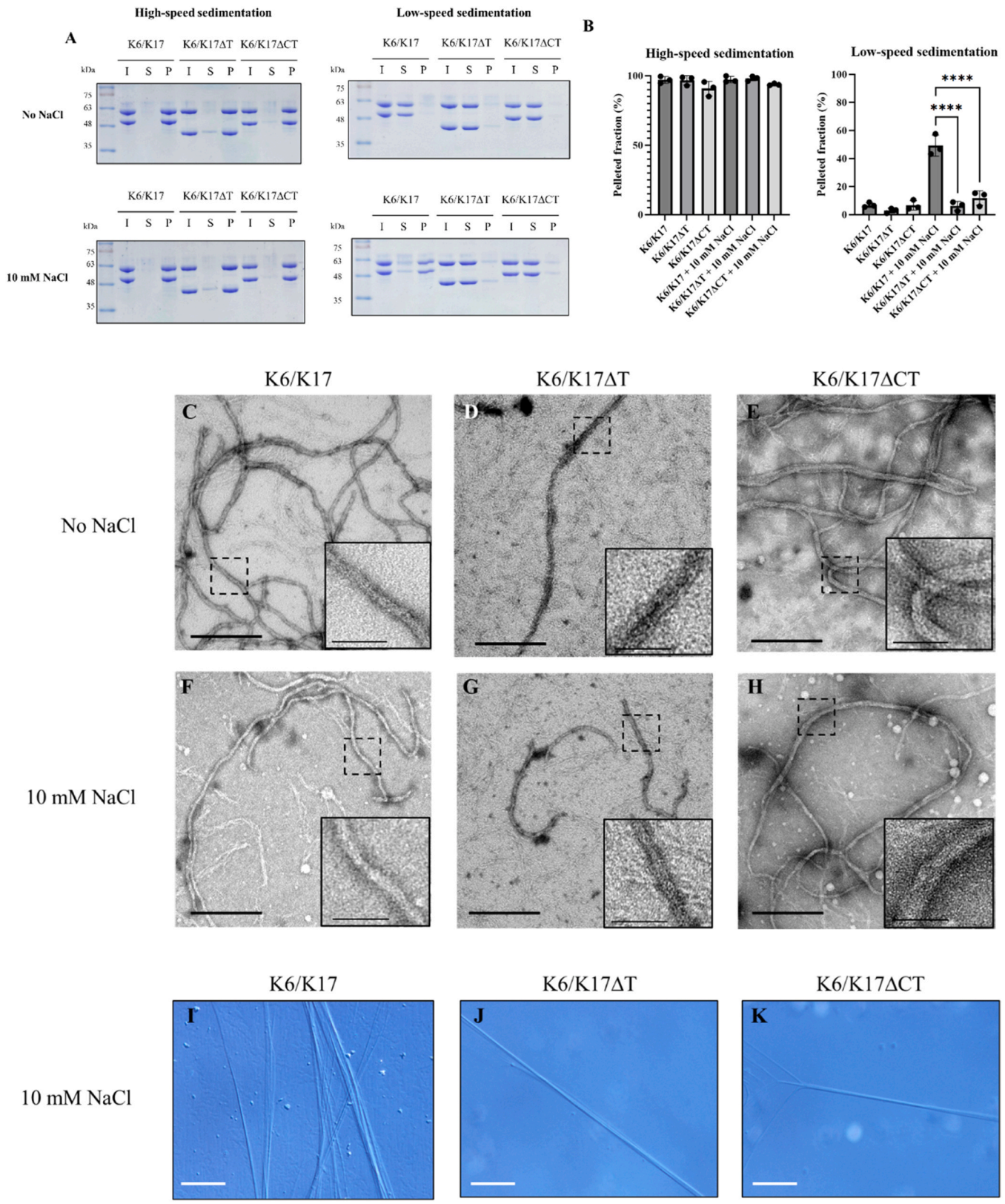

Fig. 7. Curved region in K17T plays a key role in K6/K17 filament bundling. (A) SDS-PAGE (12 % polyacrylamide gel) of the high- and low-speed sedimentation assay. I: Input; S: Supernatant; P: Pellet. (B) Densitometry-based analysis of the pelleted fractions from (A). Pellet formation represents the assembly of keratin pairs. Data indicate mean ± SD (n = 3 per group). Pellet formation represents the bundling of keratin pairs. Data indicate mean ± SD (n = 3 per group), one-way ANOVA, **** for $P < 0.0001$. (C-H) TEM images with negative staining. (C-E) Assembled keratin filaments of K6/K17, K6/K17ΔT, and K6/K17ΔCT without NaCl. The scale bars represent 200 nm. The scale bars in inlet images represent 50 nm. (F-H) Assembled keratin filaments of K6/K17, K6/K17ΔT, and K6/K17ΔCT with 10 mM NaCl. The scale bars represent 200 nm. The scale bars in the inlet images represent 50 nm. (I-K) DIC images for bundled keratin filaments of K6/K17, K6/K17ΔT, and K6/K17ΔCT. The scale bars represent 500 μm.

interacts with the rod domain of K6.

Our structural analysis confirmed that K17T exhibits the characteristics of an IDR. TALOS-N predictions indicated that K17T lacks a well-defined secondary structure; most residues adopt a highly dynamic conformation. This structural flexibility may enhance the interactions of K17T with multiple filament units during bundling. The dynamic nature of K17T may promote flexible linker activity, accommodating different spatial arrangements of the filaments and facilitating their stabilization. The NMR studies indicate an overall flexible conformation, with a distinct, relatively ordered curved central region (T404–T410). This curved structure may serve as a key functional element stabilizing filament bundling by interacting with the rod domains. The structural flexibility and dynamic properties of K17T may be key to its ability to link adjacent filaments and stabilize bundling interactions. The presence of a short structured region (T404–T410) within an otherwise disordered domain may support the contribution of K17T to filament organization, emphasizing the importance of structural plasticity in cytoskeletal assembly. Our findings showing that removal of the T404–T410 segment from K17T results in a significant impairment in filament bundling, closely mimicking the phenotype of the tailless mutant as observed in both sedimentation assays and DIC microscopy, provides supportive evidence for this interpretation.

Securing high-resolution structural data for intermediate filaments has been a significant challenge due to their heterogeneous character and properties. In this context, the recently determined cryo-EM structure of the entire vimentin filament at 7.2 Å resolution (Eibauer et al., 2024) yielded important insights that resonate with our findings. This study revealed that vimentin's tail domains, despite being predominantly intrinsically disordered regions, play a critical role by connecting protofibrils laterally through individual contact sites, analogous to outstretched hands holding and tightening the protofibrils together. This observation reinforces the biological purpose of intrinsically disordered proteins or regions within the context of cytoskeletal organization. Although vimentin belongs to a distinct group of IFs, the function of tail domains in mediating lateral interactions and overall filament network integration may be conserved to some extent across subtypes of IF proteins. Our demonstration that the intrinsically disordered K17 tail domain is essential for K6/K17 filament bundling strongly supports this emerging paradigm, suggesting a common mechanism whereby flexible, disordered tail regions contribute fundamentally to the higher-order organization and mechanical integrity of diverse intermediate filament networks.

Funding

This work was supported by the National Research Foundation of Korea (NRF) grant funded by the Korea government (MSIT) to C.H.L [NRF-2020R1A2C1099696]; funding to J. H. K. from NRF [NRF-2020R1I1A2074335]; and funding to Y. H. K. from Institute for Basic Science of Korea (IBS) [IBS-R034-D1]. P.A.C. was supported from R01 grant AR079418 from the National Institutes of Health (USA). The purchase of the software licenses, including PyMOL, was supported by the DGIST Supercomputing AI Education and Research Center.

CRediT authorship contribution statement

Pierre A. Coulombe: Writing – review & editing, Writing – original draft, Resources, Conceptualization. **Chang-Hun Lee:** Writing – review & editing, Writing – original draft, Validation, Supervision, Resources, Project administration, Investigation, Funding acquisition, Data curation, Conceptualization. **Jiwoo Yeom:** Writing – review & editing, Writing – original draft, Visualization, Methodology, Investigation. **Sanghoon Lee:** Visualization, Resources, Methodology. **Young Ho Ko:** Visualization, Resources, Methodology, Funding acquisition. **Eunmi Hong:** Visualization, Resources, Methodology. **Jin Hae Kim:** Writing – review & editing, Visualization, Validation, Resources, Methodology, Funding acquisition.

Declaration of Generative AI and AI-assisted technologies in the writing process

The writing process of this paper do not contain any technology using generative AI or AI-assisted technology.

Declaration of Competing Interest

The authors declare that they have no known competing financial interests or personal relationships that could have appeared to influence the work reported in this paper.

Acknowledgments

The authors appreciate Dr. Ji Young Mun for her efforts and intensive discussion to obtain the TEM images of keratin filaments in this work. TEM was supported by Brain Research Core Facilities in KBRI. The authors also wish to extend their sincere gratitude to Prof. Young-Sam Lee and Jinju Jeong for their insightful advice and valuable discussions throughout this research. The authors gratefully acknowledge the use of the NMR facilities at Pohang University of Science and Technology (Pohang, Republic of Korea).

Data availability

Data will be made available on request.

References

Alvarado, D.M., Coulombe, P.A., 2014. Directed expression of a chimeric type II keratin partially rescues keratin 5-null mice. J. Biol. Chem. 289 (28), 19435–19447. https://doi.org/10.1074/jbc.M114.553867.

Babu, S., Mockler, D.C., Roa-Peña, L., Szygalowicz, A., Kim, N.W., Jahanfard, S., Gholami, S.S., Moffitt, R., Fitzgerald, J.P., Escobar-Hoyos, L.F., Shroyer, K.R., 2019. Keratin 17 is a sensitive and specific biomarker of urothelial neoplasia. Mod. Pathol. 32 (5), 717–724. https://doi.org/10.1038/s41379-018-0177-5.

Baraks, G., Tseng, R., Pan, C.H., Kasliwal, S., Leiton, C.V., Shroyer, K.R., Escobar-Hoyos, L.F., 2022. Dissecting the oncogenic roles of keratin 17 in the hallmarks of cancer. Cancer Res 82 (7), 1159–1166. https://doi.org/10.1158/0008-5472.CAN-21-2522.

Bernot, K.M., Lee, C.H., Coulombe, P.A., 2005. A small surface hydrophobic stripe in the coiled-coil domain of type I keratins mediates tetramer stability. J. Cell Biol. 168 (6), 965–974. https://doi.org/10.1083/jcb.200408116.

Bousquet, O., Ma, L., Yamada, S., Gu, C., Idei, T., Takahashi, K., Wirtz, D., Coulombe, P. A., 2001. The nonhelical tail domain of keratin 14 promotes filament bundling and enhances the mechanical properties of keratin intermediate filaments in vitro. J. Cell Biol. 155 (5), 747–754. https://doi.org/10.1083/jcb.200104063.

Bunick, C.G., Milstone, L.M., 2017. The X-ray crystal structure of the keratin 1-keratin 10 helix 2B heterodimer reveals molecular surface properties and biochemical insights into human skin disease. J. Invest Dermatol. 137 (1), 142–150. https://doi.org/10.1016/j.jid.2016.08.018.

Chung, B.M., Rotty, J.D., Coulombe, P.A., 2013. Networking galore: intermediate filaments and cell migration. Curr. Opin. Cell Biol. 25 (5), 600–612. https://doi.org/10.1016/j.ceb.2013.06.007.

Cohen, E., Johnson, C., Redmond, C.J., Nair, R.R., Coulombe, P.A., 2022. Revisiting the significance of keratin expression in complex epithelia. J. Cell Sci. 135 (20), jcs260594. https://doi.org/10.1242/jcs.260594.

Cohen, E., Johnson, C.N., Wasikowski, R., Billi, A.C., Tsoi, L.C., Kahlenberg, J.M., Gudjonsson, J.E., Coulombe, P.A., 2024. Significance of stress keratin expression in normal and diseased epithelia. iScience 27 (2), 108805. https://doi.org/10.1016/j.isci.2024.108805.

Coulombe, P.A., Omary, M.B., 2002. Hard' and 'soft' principles defining the structure, function and regulation of keratin intermediate filaments. Curr. Opin. Cell Biol. 14 (1), 110–122. https://doi.org/10.1016/s0955-0674(01)00301-5.

Coulombe, P.A., Wong, P., 2004. Cytoplasmic intermediate filaments revealed as dynamic and multipurpose scaffolds. Nat. Cell Biol. 6 (8), 699–706. https://doi.org/10.1038/ncb0804-699.

Coulombe, P.A., Pineda, C.M., Jacob, J.T., Nair, R.R., 2024. Nuclear roles for non-lamin intermediate filament proteins. Curr. Opin. Cell Biol. 86, 102303. https://doi.org/10.1016/j.ceb.2023.102303.

DeLano, W.L., 2002. Pymol: an open-source molecular graphics tool. CCP4 Newsl. Protein Crystallogr. 40 (1), 82–92.

Delgado-Coka, L.A., Roa-Peña, L., Babu, S., Horowitz, M., Petricoin 3rd., E.F., Matrisian, L.M., Blais, E.M., Marchenko, N., Allard, F.D., Akalin, A., Jiang, W., Larson, B.K., Hendifar, A.E., Picozzi, V.J., Choi, M., Shroyer, K.R., Escobar-Hoyos, L.

F., 2024. Keratin 17 is a prognostic and predictive biomarker in pancreatic ductal adenocarcinoma. Am. J. Clin. Pathol. 162 (3), 314–326. https://doi.org/10.1093/ajcp/aqae038.
Eibauer, M., Weber, M.S., Kronenberg-Tenga, R., et al., 2024. Vimentin filaments integrate low-complexity domains in a complex helical structure. Nat. Struct. Mol. Biol. 31, 939–949. https://doi.org/10.1038/s41594-024-01261-2.
Eldirany, S.A., Ho, M., Hinbest, A.J., Lomakin, I.B., Bunick, C.G., 2019. Human keratin 1/10-1B tetramer structures reveal a knob-pocket mechanism in intermediate filament assembly. EMBO J. 38 (11), e100741. https://doi.org/10.15252/embj.2018100741.
Franke, W.W., 1987. Homology of a conserved sequence in the tail domain of intermediate filament proteins with the loop region of calcium binding proteins. Cell Biol. Int Rep. 11 (11), 831. https://doi.org/10.1016/0309-1651(87)90163-9.
Fuchs, E., Cleveland, D.W., 1998. A structural scaffolding of intermediate filaments in health and disease. Science 279 (5350), 514–519. https://doi.org/10.1126/science.279.5350.514.
Fuchs, E., Weber, K., 1994. Intermediate filaments: structure, dynamics, function, and disease. Annu Rev. Biochem 63, 345–382. https://doi.org/10.1146/annurev.bi.63.070194.002021.
Fukuyama, K., Murozuka, T., Caldwell, R., Epstein, W.L., 1978. Divalent cation stimulation of in vitro fibre assembly from epidermal keratin protein. J. Cell Sci. 33, 255–263. https://doi.org/10.1242/jcs.33.1.255. PMID: 569162.
Gass, J.K., Wilson, N.J., Smith, F.J.D., Lane, E.B., McLean, W.H.I., Rytina, E., Salvary, I., Burrows, N.P., 2009. Steatocystoma multiplex, oligodontia and partial persistent primary dentition associated with a novel keratin 17 mutation. Br. J. Dermatol. 161 (6), 1396–1398. https://doi.org/10.1111/j.1365-2133.2009.09383.x.
Geisbrecht, B.V., Bouyain, S., Pop, M., 2006. An optimized system for expression and purification of secreted bacterial proteins. Protein Expr. Purif. 46 (1), 23–32. https://doi.org/10.1016/j.pep.2005.09.003.
Hobbs, R.P., Batazzi, A.S., Han, M.C., Coulombe, P.A., 2016. Loss of keratin 17 induces tissue-specific cytokine polarization and cellular differentiation in HPV16-driven cervical tumorigenesis in vivo. Oncogene 35 (43), 5653–5662. https://doi.org/10.1038/onc.2016.102.
Khanom, R., Nguyen, C.T.K., Kayamori, K., Zhao, X., Morita, K., Miki, Y., et al., 2016. Keratin 17 is induced in oral cancer and facilitates tumor growth. PLoS One 11 (8), e0161163. https://doi.org/10.1371/journal.pone.0161163.
Kim, S., Coulombe, P.A., 2007. Intermediate filament scaffolds fulfill mechanical, organizational, and signaling functions in the cytoplasm. Genes Dev. 21 (13), 1581–1597. https://doi.org/10.1101/gad.1552107.
Kim, S., Wong, P., Coulombe, P.A., 2006. A keratin cytoskeletal protein regulates protein synthesis and epithelial cell growth. Nature 441 (7091), 362–365. https://doi.org/10.1038/nature04659.
Lee, C.H., Coulombe, P.A., 2009. Self-organization of keratin intermediate filaments into cross-linked networks. J. Cell Biol. 186 (3), 409–421. https://doi.org/10.1083/jcb.200810196.
Lee, C.H., Kim, M.S., Chung, B.M., Leahy, D.J., Coulombe, P.A., 2012. Structural basis for heteromeric assembly and perinuclear organization of keratin filaments. Nat. Struct. Mol. Biol. 19 (6), 707–715. https://doi.org/10.1038/nsmb.2330.
Lee, C.H., Kim, M.S., Li, S., Leahy, D.J., Coulombe, P.A., 2020. Structure-function analyses of a keratin heterotypic complex identify specific keratin regions involved in intermediate filament assembly. Structure 28 (3), 355–362.e4. https://doi.org/10.1016/j.str.2020.01.002.
Lee, W., Petit, C.M., Cornilescu, G., Stark, J.L., Markley, J.L., 2016. The AUDANA algorithm for automated protein 3D structure determination from NMR NOE data. J. Biomol. NMR 65, 51–57. https://doi.org/10.1007/s10858-016-0036-y.
Lee, W., Rahimi, M., Lee, Y., Chiu, A., 2021. POKY: a software suite for multidimensional NMR and 3D structure calculation of biomolecules. Bioinformatics 37 (18), 3041–3042. https://doi.org/10.1093/bioinformatics/btab180.
Liao, H., Sayers, J.M., Wilson, N.J., Irvine, A.D., Mellerio, J.E., Baselga, E., et al., 2007. A spectrum of mutations in keratins K6a, K16, and K17 causing pachyonychia congenita. J. Dermatol. Sci. 48 (3), 199–205. https://doi.org/10.1016/j.jdermsci.2007.07.003.
Lin, Y., Zhang, W., Li, B., Wang, G., 2022. Keratin 17 in psoriasis: current understanding and future perspectives. Semin Cell Dev. Biol. 128, 112–119. https://doi.org/10.1016/j.semcdb.2021.06.018.
Liu, Z., Yu, S., Ye, S., Shen, Z., Gao, L., Han, Z., Zhang, P., Luo, F., Chen, S., Kang, M., 2020. Keratin 17 activates AKT signalling and induces epithelial-mesenchymal transition in oesophageal squamous cell carcinoma. J. Proteom. 211, 103557. https://doi.org/10.1016/j.jprot.2019.103557.
Ma, L., Yamada, S., Wirtz, D., Coulombe, P.A., 2001. A 'hot-spot' mutation alters the mechanical properties of keratin filament networks. Nat. Cell Biol. 3 (5), 503–506. https://doi.org/10.1038/35074576.
McGowan, K., Coulombe, P.A., 1998. The wound repair-associated keratins 6, 16, and 17. Insights into the role of intermediate filaments in specifying keratinocyte cytoarchitecture. Subcell. Biochem 31, 173–204.
McLean, W.H., Lane, E.B., 1995. Intermediate filaments in disease. Curr. Opin. Cell Biol. 7 (1), 118–125. https://doi.org/10.1016/0955-0674(95)80053-0.
Omary, M.B., Coulombe, P.A., McLean, W.H.I., 2004. Intermediate filament proteins and their associated diseases. N. Engl. J. Med 351 (20), 2087–2100. https://doi.org/10.1056/NEJMra040319.
Peck, Y., Pickering, D., Mobli, M., Liddell, M.J., Wilson, D.T., Ruscher, R., Ryan, S., Buitrago, G., McHugh, C., Love, N.C., Pinlac, T., Haertlein, M., Kron, M.A., Loukas, A., Daly, N.L., 2024. Solution structure of the N-terminal extension domain of a *schistosoma japonicum* asparaginyl-tRNA synthetase. J. Biomol. Struct. Dyn. 42 (15), 7934–7944. https://doi.org/10.1080/07391102.2023.2241918.
Pegoraro, A.F., Janmey, P., Weitz, D.A., 2017. Mechanical properties of the cytoskeleton and cells. Cold Spring Harb. Perspect. Biol. 9 (11), a022038. https://doi.org/10.1101/cshperspect.a022038.
Ramms, L., Fabris, G., Windoffer, R., Schwarz, N., Springer, R., Zhou, C., Lazar, J., Stiefel, S., Hersch, N., Schnakenberg, U., Magin, T.M., Leube, R.E., Merkel, R., Hoffmann, B., 2013. Keratins as the main component for the mechanical integrity of keratinocytes. Proc. Natl. Acad. Sci. USA 110 (46), 18513–18518. https://doi.org/10.1073/pnas.1313491110.
Roa-Peña, L., Leiton, C.V., Babu, S., Pan, C.H., Vanner, E.A., Akalin, A., Bandovic, J., Moffitt, R.A., Shroyer, K.R., Escobar-Hoyos, L.F., 2019. Keratin 17 identifies the most lethal molecular subtype of pancreatic cancer. Sci. Rep. 9 (1), 11239. https://doi.org/10.1038/s41598-019-47519-4.
Schwieters, C.D., Kuszewski, J., Clore, G.M., 2006. Using Xplor-NIH for NMR molecular structure determination. Prog. Nucl. Magn. Reson Spectrosc. 48, 47–62. https://doi.org/10.1016/j.pnmrs.2005.10.001.
Seltmann, K., Fritsch, A.W., Kas, J.A., Magin, T.M., 2013. Keratin significantly contributes to cell stiffness and impacts invasive behavior. Proc. Natl. Acad. Sci. USA 110 (46), 18507–18512. https://doi.org/10.1073/pnas.1310493110.
Shen, Y., Bax, A., 2015. Protein structural information derived from NMR chemical shift with the neural network program TALOS-N. Methods Mol. Biol. 1260, 17–32. https://doi.org/10.1007/978-1-4939-2239-0_2.
Tong, X., Coulombe, P.A., 2006. Keratin 17 modulates hair follicle cycling in a TNFalpha-dependent fashion. Genes Dev. 20 (10), 1353–1364. https://doi.org/10.1101/gad.1387406.
Wilson, A.K., Coulombe, P.A., Fuchs, E., 1992. The roles of K5 and K14 head, tail, and R/K L L E G E domains in keratin filament assembly in vitro. J. Cell Biol. 119 (2), 401–414. https://doi.org/10.1083/jcb.119.2.401.
Windoffer, R., Beil, M., Magin, T.M., Leube, R.E., 2011. Cytoskeleton in motion: the dynamics of keratin intermediate filaments in epithelia. J. Cell Biol. 194 (5), 669–678. https://doi.org/10.1083/jcb.201008095.
Wu, H., Shen, Y., Wang, D., Herrmann, H., Goldman, R.D., Weitz, D.A., 2020. Effect of divalent cations on the structure and mechanics of vimentin intermediate fialments. Biophys. J. 119 (1), 55–64. https://doi.org/10.1016/j.bpj.2020.05.016.
Xu, Y., Cohen, E., Johnson, C.N., Parent, C.A., Coulombe, P.A., 2024. Repeated stress to the skin amplifies neutrophil infiltration in a keratin 17- and PKCα-dependent manner. PLoS Biol. 22 (8), e3002779. https://doi.org/10.1371/journal.pbio.3002779.
Yamada, S., Wirtz, D., Coulombe, P.,A., 2002. Pairwise assembly determines the intrinsic potential for self-organization and mechanical properties of keratin filaments. Mol. Biol. Cell 13 (1), 382–391. https://doi.org/10.1091/mbc.01-10-0522.
Yang, L., Zhang, S., Wang, G., 2018. Keratin 17 in disease pathogenesis: from cancer to dermatoses. J. Pathol. 247 (2), 158–165. https://doi.org/10.1002/path.5178.
Zhang, X., Yin, M., Zhang, L.J., 2019. Keratin 6, 16 and 17 – critical barrier alarmin molecules in skin wounds and psoriasis. Cells 8 (8), 807. https://doi.org/10.3390/cells8080807.
Zieman, A.G., Coulombe, P.A., 2020. A study of the rare disease pachyonychia congenita (PC). Br. J. Dermatol. 182 (3), 564–573. https://doi.org/10.1111/bjd.18033.